J. Chem. Sci. Vol. 129, No. 11, November 2017, pp. 1787–1794.
https://doi.org/10.1007/s12039-017-1359-2

REGULAR ARTICLE

Special Issue on Recent Trends in the Design and Development of Catalysts and their Applications

Syngas production by CO_2 reforming of methane on $LaNi_xAl_{1-x}O_3$ perovskite catalysts: influence of method of preparation

T V SAGAR[a], D PADMAKAR[a], N LINGAIAH[a], K S RAMA RAO[a], I A K REDDY[b] and P S SAI PRASAD[a,*]

[a]CSIR-Indian Institute of Chemical Technology (CSIR-IICT), Hyderabad, Telangana 500 007, India
[b]Chemistry Department, National Institute of Technology, Warangal, Telangana 506 004, India
E-mail: saiprasad@iict.res.in

MS received 15 April 2017; accepted 24 July 2017; published online 21 September 2017

Abstract. Two series of $LaNi_xAl_{1-x}O_3$ catalysts ($0 \leq x \leq 1$) were prepared by hydrothermal and sol–gel methods and characterized by X-ray diffraction (XRD), BET surface area, Temperature programmed reduction (TPR) and Fourier- transform infrared spectroscopy (FT-IR) techniques. The performance of these catalysts was studied for CO_2 reforming of methane (also called dry reforming of methane, DRM) at atmospheric pressure and in the temperature range of 600−800°C, maintaining a space velocity of 28,800 h^{-1}. Catalysts containing trimetallic perovskite showed higher CH_4 and CO_2 conversions than the bimetallic perovskite, due to the strong interaction of Ni with the former. Strong interaction increased the reduction temperature of the active species and reduced the sintering of metallic particles. At 800°C, the sol–gel catalysts reached their maximum activity in terms of both CH_4 and CO_2 conversions at $x = 0.3$, whereas the same for hydrothermal catalysts required a Ni ratio $x = 0.6$. The trimetallic perovskite formation was responsible for the catalyst stability. A comparison of the best catalysts from the two series revealed that the hydrothermal catalysts exhibited a slightly better performance during the time on stream analysis. The results are interpreted in terms of changes in the physicochemical properties of the catalysts.

Keywords. CO_2 reforming of methane; La–Ni–Al perovskites; hydrothermal synthesis; sol–gel synthesis; syngas production.

1. Introduction

Climate change due to increasing concentrations of global warming gases, particularly CO_2 and CH_4 in the atmosphere is a great concern globally.[1,2] Most of the CO_2 released into the atmosphere is due to burning of fossil fuels like coal, natural gas and oil. The amount of carbon dioxide reaching the atmosphere can be minimized by different techniques such as; CO_2 capture, transportation and sequestration.[3] However, the extent of the gas emission (about 35 billion tons/year) is so high that the existing methods cannot alleviate the problem. Instead of a pollutant, carbon dioxide is now projected as a cheap and non-toxic raw material for chemical production.[4] Since the utilization of carbon dioxide in the production of chemicals like urea and salicylic acid is very limited, its transformation into fuels has attracted the attention of researchers recently.[5,6] Reforming of methane with carbon dioxide to produce syngas is a very attractive route to produce fuels and chemicals.[7] This reaction has its importance due to utilization of the two potential green house gases, methane and carbon dioxide.[8] Compared to partial oxidation and steam reforming of methane, usually operated at high temperatures and pressure,[9] CO_2 reforming of methane is easy to handle. DRM produces syngas of H_2/CO ratio 1 which is a suitable feed stack for the Fischer–Tropsch synthesis.[10–13] It has recently been used to trap solar energy also because of its high endothermicity. However, DRM has a major disadvantage of rapid catalytic deactivation due to coke formation. The carbon deposition on the active sites of catalyst is mainly due to CO disproportionation ($2CO \rightarrow CO_2 + C$; $\Delta H^\circ = -172.2$ kJ/mol) and methane decomposition ($CH_4 \rightarrow 2H_2 + C$; $\Delta H^\circ = 74.9$ kJ/mol).[14,15]

Literature reveals that the noble metals like Pd, Ru, Rh, Pt and Ir show good activity during the DRM reaction. Due to low availability and high cost, the industrialization of the technologies involving these

*For correspondence

catalysts has become a big question.[16] Non-noble metals, mostly of group VIII, are catalytically active for CH_4 reforming.[7,17] Among the non-noble metals, Ni is more economically viable as a catalyst. High turnover rates, the inherent availability, low cost and remarkable long-term stability are its advantages.[18] Metallic Ni is the active site in the DRM reaction. However, Ni in its metallic form is highly susceptible to sintering during the high-temperature reaction, which decreases the number of active sites and increases coking. Dilution of Ni by the second metal like Mn, Fe, Cu or Al has been tried with limited success. Fixing Ni in perovskites like oxides containing two or more of La, Ni, Fe and Co have been adopted as a better option for the preparation of catalysts for DRM. Unfortunately, bimetallic perovskites like $LaNiO_3$ and $LaCoO_3$ have shown a total reduction at temperatures less than that of the operating temperature of DRM, making them not suitable as stable catalysts. The application of LaNiFe or LaCoFe trimetallic perovskites has been suggested for catalyzing the reaction as they at least remain partially stable at reaction temperatures. Moradi *et al.*,[19] first studied the activity of $LaNi_xAl_{1-x}O_3$ trimetallic perovskites during the DRM reaction. They prepared the catalysts by the sol–gel method. Further studies on the effect of the method of preparation $LaNi_xAl_{1-x}O_3$ perovskites are scarce. In the present study, the catalysts were prepared by the hydrothermal method, characterized by several techniques and evaluated for the DRM reaction. Since Moradi *et al.*,[19] evaluated the catalysts under temperature programmed philosophy, a direct comparison of the performance of the present hydrothermal catalysts with their catalysts is difficult. Hence, a separate batch of catalysts was again prepared following the sol–gel route and the activities of the two types of catalysts are compared in this presentation. The changes associated with the change in method of preparation are explained in terms of their physicochemical properties.

2. Experimental

2.1 *Catalyst preparation*

Two series of $LaNi_xAl_{1-x}O_3$ perovskite catalysts with $0 \leq x \leq 1$ were prepared by the hydrothermal and sol–gel methods.[20,21] Required amounts of $La(NO_3)_3 \cdot 6H_2O$, $Ni(NO_3)_2 \cdot 6H_2O$ and $Al(NO_3)_3 \cdot 9H_2O$ (SD Fine Chemicals, India) were separately dissolved in hot propionic acid. The solutions of metal propionates of nickel and aluminium were mixed and then the mixture was added to lanthanum propionate solution. After stirring for 30 min, the solution was kept under reflux for 24 h. In the case of the sol–gel method, the paste obtained was dried under reduced pressure. The resulting solid was dried and calcined at 800°C, with a temperature ramp of 2°C/min and maintaining the same temperature for 4 h. For the hydrothermally treated catalyst preparation, the solution after reflux was transferred to an autoclave and kept at 150°C for 24 h. The resin obtained was dried under reduced pressure. The final powder sample was calcined at 800°C with a temperature ramping of 2°C/min. The quantities of metal nitrate salts were selected such that the finished catalysts had their Ni content, $x = 0, 0.2, 0.3, 0.4, 0.6, 0.8$ and 1.

2.2 *Catalyst characterization*

BET surface areas were determined by N_2 adsorption on a SMART SORB 92/93 instrument (M/s. SMART Instruments, India). Prior to BET measurements, the samples were subjected to degasification at 150°C for 2 h. The XRD patterns of the catalysts were obtained on an Ultima-IV diffractometer (M/s. Rigaku Corporation, Japan) using nickel-filtered Cu K α radiation ($\lambda = 1.54$Å). The measurements were recorded in steps of 0.045° and a count time of 0.5 s in the 2θ range of 10 to 60°. Identification of the crystalline phases was carried out with the help of JCPDS files. TPR studies were performed using a homemade apparatus. Catalyst sample (50 mg) taken in a quartz reactor was reduced under $10\%H_2/Ar$ gas mixture flowing at 30 ml/min with a heating rate of 5°C/min up to 800°C. After reaching the final temperature, the catalyst was kept under the isothermal condition for 1 h. Before the TPR run, the catalyst was pretreated in Ar flow at 300°C for 2 h. The hydrogen consumption was monitored using thermal conductivity detector of a gas chromatograph (Varian, 8301). FT-IR spectra were recorded using the KBr pellet method on a Perkin Elmer (Spectrum GX, USA) instrument.

2.3 *Activity test*

DRM reaction studies were conducted in a fixed bed reactor at atmospheric pressure, in the temperature range of 600−800°C maintaining a space velocity of $28,800\ h^{-1}$. 0.5 g of catalyst mixed with 0.5 g of ceramic beads was suspended in the middle of the reactor between two quartz plugs. Prior to the activity measurements, the sample was reduced *in situ* under 60% H_2 balanced N_2 gas mixture at 600°C for 6 h. After attaining the required temperature, the reaction was conducted for a period of 1 h to attain steady-state. The product was analyzed online on a Nucon 5765 gas chromatograph equipped with a carbosphere column using Ar gas as a carrier and a TC detector. The values provided here are the average values of two analyses carried for 1 h each. The accuracy was within the error margin of ±2%.

3. Results and Discussion

3.1 *Specific surface area*

Table 1 shows the specific surface areas of the calcined catalysts. Low values of specific surface areas were

Table 1. Specific surface areas of the catalysts.

S. no.	Catalyst	Specific surface area (m^2/g)	
		Hydrothermal	Sol–gel
1	$LaNi_{0.2}Al_{0.8}O_3$	13.6	11.2
2	$LaNi_{0.3}Al_{0.7}O_3$	11.2	17.7
3	$LaNi_{0.4}Al_{0.6}O_3$	10.2	18.6
4	$LaNi_{0.6}Al_{0.4}O_3$	9.6	9.6
5	$LaNi_{0.8}Al_{0.2}O_3$	1.9	1.9

recorded for both the series of catalysts. It is known that the surface area of a catalyst is highly dependent on its calcination temperature.[22] High calcination temperature might be the reason for the low surface areas. According to Khalesi *et al.*,[23] low surface area materials are more favourable for DRM as they suppress the side reactions.[23]

3.2 *X-ray diffraction studies*

XRD patterns of the hydrothermal catalysts are shown in Figure 1A. The patterns were dominated by peaks due to perovskite phases. With the increase in active metal (Ni) ratio peak shifting from $2\theta = 33.34°$ ($LaAlO_3$) to 32.92° ($LaNiO_3$) was observed (Figure 2A), as also reported by Moradi *et al.*[19] This testifies the formation of the trimetallic $LaNi_xAl_{1-x}O_3$ perovskites. In low Ni content catalysts, no other phase was observed. At high Ni content, the catalysts showed the presence of individual metal oxides also. In the catalyst with x = 0.8, the observed peaks at $2\theta = 27.92$, 39.54, 48.77, 55.31 and 59.31° revealed the formation of monoclinic La_2O_3 (JCPDS-220641), at $2\theta = 27.28$ and 31.7° the cubic La_2O_3 (JCPDS-220369) and at $2\theta = 43.21$ and 37.27° the NiO (JCPDS-780643) formation.

The XRD patterns of the sol–gel catalysts are shown in Figure 1B. The sol–gel method also yielded the perovskite phases. All the catalysts showed bi- and trimetallic perovskite phases. Again, by changing the active metal (Ni) ratio from x= 1 to 0, the peak at $2\theta = 32.92°$ ($LaNiO_3$) shifted to 33.34° ($LaAlO_3$) confirming the formation of trimetallic perovskites (Figure 2B) in the intermediate region of x. More number of diffraction peaks were observed for the catalyst with x = 0.8. These peaks indicated the presence of La_2O_3. The essential difference between the two series of catalysts can be seen from the curves displayed in Figure 3. For the same change in the lattice parameter higher Ni ratio was required in the case of hydrothermal catalysts. Alternatively, for the same extent of Ni incorporation in the trimetallic catalyst, the initial requirement of Ni

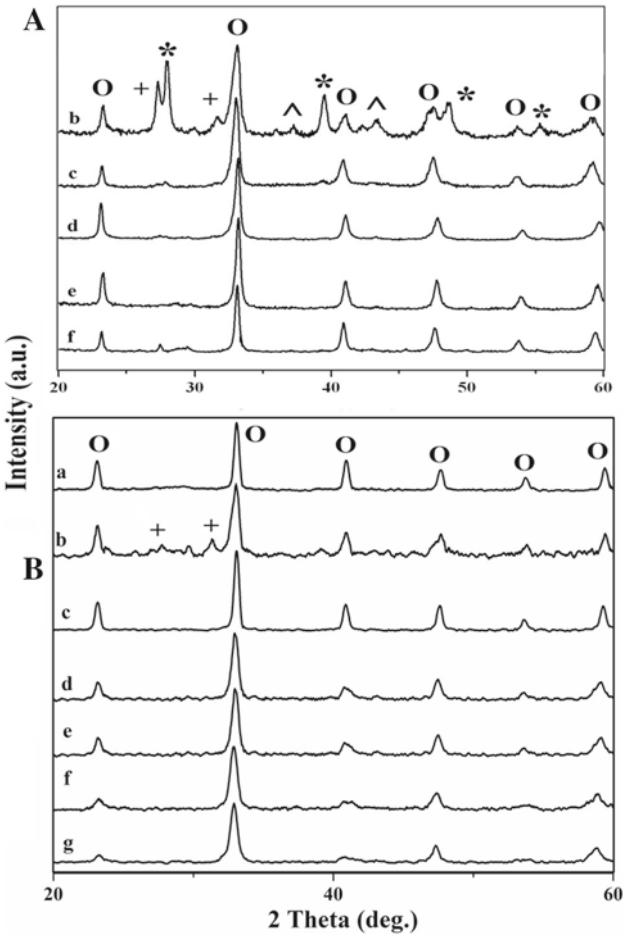

Figure 1. X-ray patterns of $LaNi_xAl_{1-x}O_3$ catalysts prepared by (A) Hydrothermal method; (B) Sol–gel method. (a) $x = 1$; (b) $x = 0.8$; (c) $x = 0.6$; (d) $x = 0.4$; (e) $x = 0.3$; (f) $x = 0.2$; and (g) $x = 0$. (*) Monoclinic La_2O_3, (+) cubic La_2O_3, (O) perovskite (a = $LaNiO_3$, g = $LaAlO_3$), (^) NiO.

was more. That means more Ni was in strong interaction with the trimetallic perovskite.

3.3 *Temperature programmed reduction*

DRM is a metal active reaction.[24,25] Strong interaction between the reduced metal and the perovskite structure is required to prevent sintering of the metal particles.[19] So, attention was focused on the reducibility of catalysts. Figure 4A shows H_2-TPR patterns of hydrothermally prepared $LaNi_xAl_{1-x}O_3$ perovskite catalysts. The patterns were characterized by the presence of peaks with maxima appearing in two zones; the first low-temperature zone falling in the temperature region of 350−500°C, and the second high-temperature zone falling in between 600 and 800°C. The first zone contains either a single or a doublet peak representing either

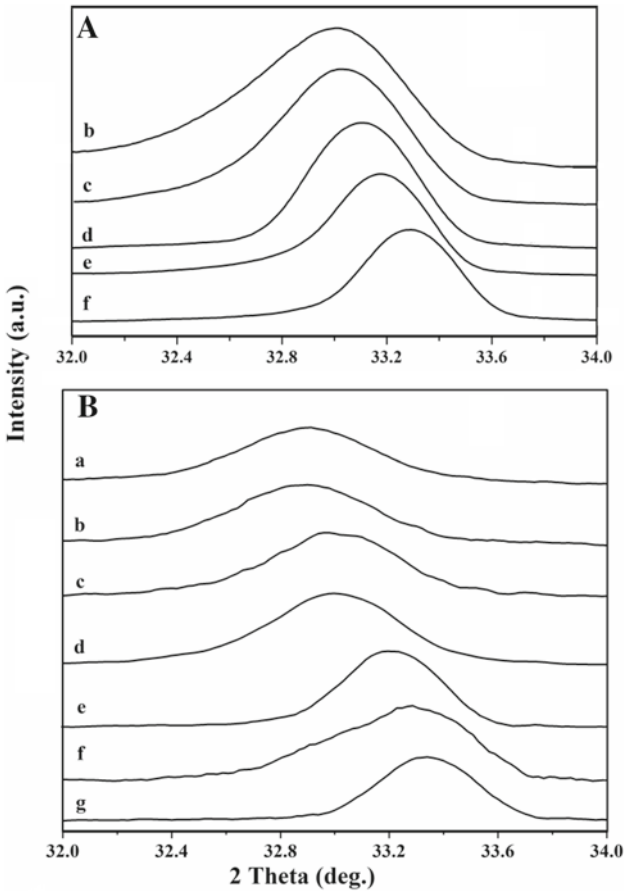

Figure 2. Expanded zone of 2θ in the X-ray patterns of $LaNi_xAl_{1-x}O_3$ catalysts prepared by (A) Hydrothermal method; (B) Sol–gel method. (a) $x = 1$; (b) $x = 0.8$; (c) $x = 0.6$; (d) $x = 0.4$; (e) $x = 0.3$; (f) $x = 0.2$; and (g) $x = 0$.

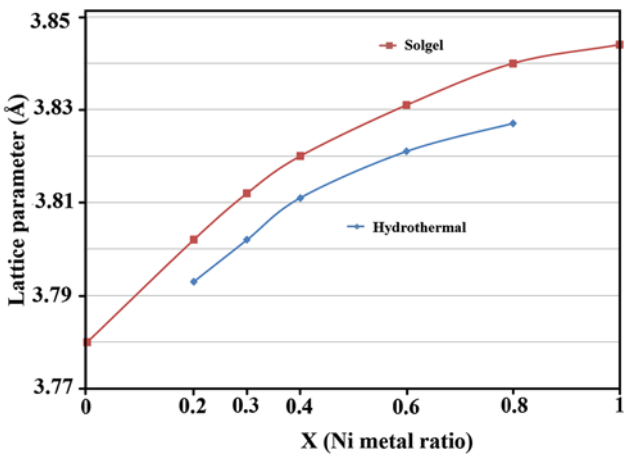

Figure 3. Change in lattice parameter of $LaNi_xAl_{1-x}O_3$ catalysts prepared by Hydrothermal and Sol–gel methods.

a direct reduction of Ni^{3+} in $LaNiO_3$ to Ni^0 or by a two-stage process represented by the following equations:

$$2LaNiO_3 + H_2 \rightarrow La_2Ni_2O_5 + H_2O \quad (1)$$

$$La_2Ni_2O_5 + 2H_2 \rightarrow La_2O_3 + 2Ni + 2H_2O \quad (2)$$

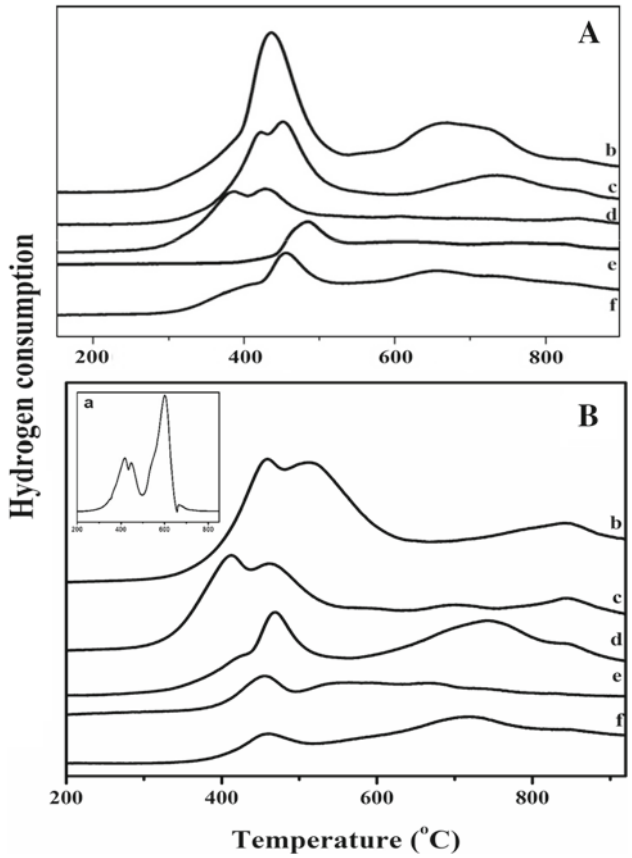

Figure 4. TPR profiles of $LaNi_xAl_{1-x}O_3$ catalysts prepared by (A) Hydrothermal method; (B) Sol–gel method. (a) $x = 1$; (b) $x = 0.8$; (c) $x = 0.6$; (d) $x = 0.4$; (e) $x = 0.3$ and (f) $x = 0.2$.

However, the inset figure corresponding to pure $LaNiO_3$ (x = 1), shows two major reduction zones; the first zone at ~450°C representing the reduction of Ni^{3+} to Ni^{2+} and second zone at ~600°C indicating the reduction of Ni^{2+} species in the brownmillerite phase to Ni^0.[26] The homogeneous formation of $LaNiO_3$ can be estimated with the intensities of first and second peaks. The intensity of the second peak equals to twice that of the first peak indicating the formation of $LaNiO_3$.[26–29] The appearance of the second zone peak between 600 and 800°C in the catalysts demonstrates the interaction of the Ni with the trimetallic perovskite phase indirectly pointing to the stability of the perovskite.[19,25,30] It can be clearly noted from the figure that the high-temperature peak shifted to its right when compared to that in the inset $LaNiO_3$, indicating the formation of trimetallic perovskite phase. This study is in good correlation with the XRD studies confirming the formation of trimetallic perovskites.

The sol–gel catalysts (Figure 4B) also exhibited similar reduction patterns as those of the hydrothermal catalysts. The low and high-temperature peaks were observed. A clear distinction between the reduction

peaks of the two series of catalysts was that the high-temperature reduction peaks indicating the trimetallic perovskite phase formation were clearer in the hydrothermal catalysts, particularly in the high Ni containing catalysts than those in the sol–gel catalysts.

3.4 *Fourier-transform infrared spectroscopy*

FT-IR spectra of the hydrothermally prepared $LaNi_xAl_{1-x}O_3$ perovskites are presented in Figure 5A. These bands can be divided into four zones, with 2–3 peaks in each zone. In the first zone, the band at ~3500 cm^{-1} is associated with the O–H stretch of intermolecular hydrogen bonds or molecular water. In the second zone, strong and sharp absorption bands appearing at ~1484 and ~1382 cm^{-1} can be ascribed to the asymmetric and symmetric COO^- stretching modes of the coordinated carboxylate groups existing even after high-temperature calcination, as also observed by Moradi *et al.*,[19] in their studies on La–Ni–Al perovskite catalysts prepared by sol–gel method. The third zone, comprises three absorption bands at ~1187, 1103 and 1063 cm^{-1} corresponding to the Al–OH bending mode.[31,32] With the increase in the Ni ratio the bands related to Al–OH decreased in their intensity. In the fourth zone, the two absorption peaks appearing at ~678 and 436 cm^{-1} can be assigned to AlO_6 octahedral in $LaAlO_3$.[33] Zhou *et al.*,[31] in their studies on $LaAlO_3$ prepared by EDTA method, observed bands related to $LaAlO_3$ at 440 and 656 cm^{-1}. In the present study, these peaks decreased in their intensity considerably with an increase in Ni ratio. Small traces of nitrates were also observed in low Ni containing catalysts with peaks at ~870 and 807 cm^{-1}.

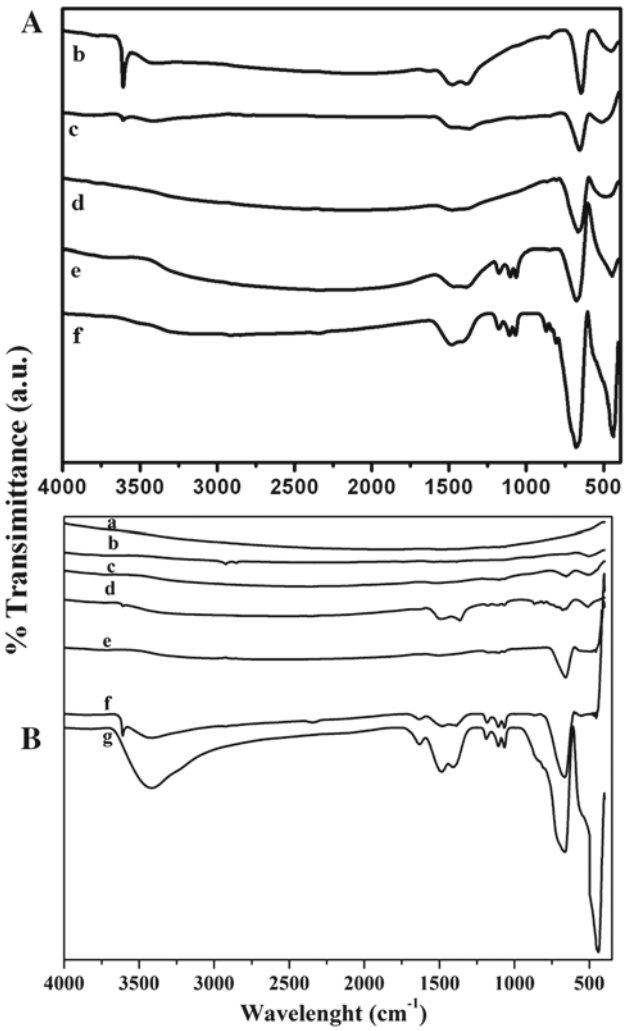

Figure 5. FT-IR profiles of $LaNi_xAl_{1-x}O_3$ catalysts. (a) x = 1; (b) $x = 0.8$; (c) $x = 0.6$; (d) $x = 0.4$; (e) $x = 0.3$; (f) $x = 0.2$ and (g) x = 0.

The vibrational bands in the FT-IR spectra of the sol–gel $LaNi_xAl_{1-x}O_3$ oxides are presented in Figure 5B. The peaks related to O–H stretching bands of inter layer molecular water at 3400 cm^{-1} appeared clearly only with x = 0.1 catalyst, whereas in the other catalysts it was not identified. The strong and sharp absorption bands at ~1680, 1484 and 1382 cm^{-1}, can be ascribed to the asymmetric and symmetric COO^- stretching modes of the coordinated carboxylate groups,[19] which disappeared slowly with the addition of Ni. The absorption bands at ~1187, 1103 and 1063 cm^{-1} correspond to the Al–OH bending mode.[31] These bands also vanished with high Ni addition more than x = 0.2. The addition of active metal, Ni to $LaAlO_3$ perovskite phase takes place by the incorporation of Ni into the lattice. This reduces the formation of inter layer water molecules and the Al – OH bands. Two absorption bands appeared with peaks at ~678 and 436 cm^{-1} corresponding to AlO_6 octahedra in $LaAlO_3$.[31,33] These peaks also disappeared with the addition of Ni. The main observation in the hydrothermal catalysts was that it helped diminish the Al-OH and propionate residues after calcination.

3.5 *Activity of the catalysts*

Figure 6 illustrates the variation of conversions at 800°C and syngas ratio with respect to Ni content on the hydrothermal and sol–gel catalysts. In the case of hydrothermal catalysts (Figure 6A) the conversions of CH_4 and CO_2 increased with increase in Ni ratio from 0.2 to 0.6. On the x = 0.6 catalyst, the conversions of CH_4 and CO_2 attained their maximum values of 94 and 97%, respectively. The increase in Ni content increased the syngas ratio also reaching the maximum value of 0.98 on x = 0.6 catalyst. This value is close to the theoretical value of 1 considering the reaction stoichiometry ($CH_4 + CO_2 \rightarrow 2H_2 + 2CO$ ($H_2/CO = 1$)).

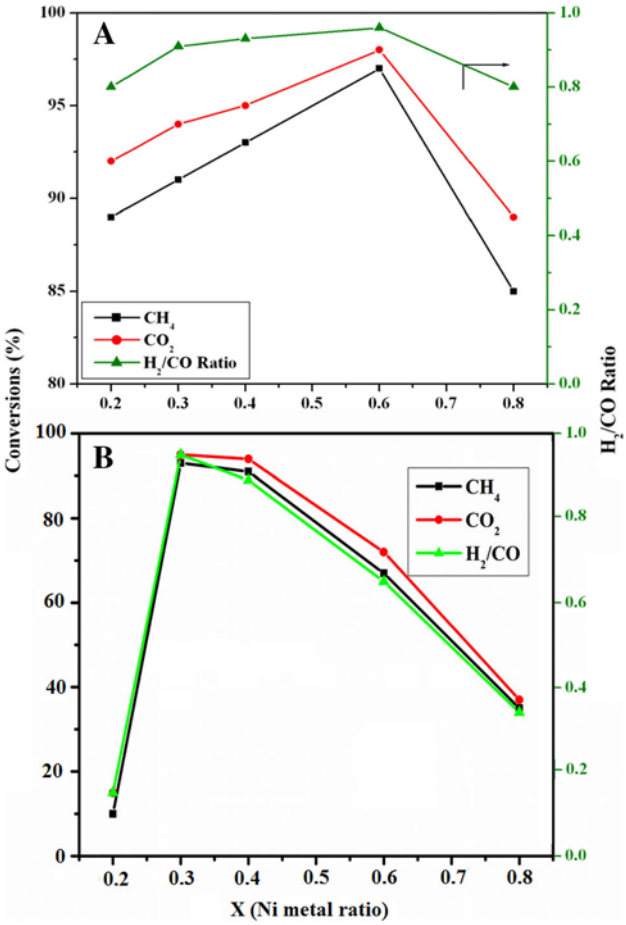

Figure 6. Change in conversions and syngas ratio with a change in Ni metal ratio in $LaNi_xAl_{1-x}O_3$ catalysts prepared by (A) Hydrothermal method; (B) Sol–gel method.

The activity profiles of the sol–gel catalysts, observed during the dry reforming reaction, expressed as a variation in their CH_4 and CO_2 conversion with the Ni content are displayed in Figure 6B. The conversions increased with Ni content, as in the case of hydrothermal catalysts. However, the increase was seen till x = 0.3 and then they started decreasing. CH_4 and CO_2 conversions reached 93 and 96%, respectively for the x = 0.3 catalyst. The H_2/CO ratio in the syngas reached a maximum value of 0.97 for the same catalyst.

According to the characterization study, the formation of trimetallic perovskite phase increased with increase in Ni ratio. At the highest Ni ratio (x = 1) the XRD showed the bimetallic $LaNiO_3$ perovskite formation and when x = 0 the patterns showed $LaAlO_3$ formation. In the case of catalysts with intermediate x values, the XRD displayed the presence of the trimetallic perovskite formation, confirmed by the shift in the characteristic peaks. These changes were also reflected in the reduction behavior of the catalysts. The formation of such trimetallic spices yields high dispersed Ni, increasing the catalytic activity.

The trimetallic perovskite completely reduces at temperatures higher than the reaction temperature. Thus, they exist in the partially reduced state. Strong metal-structure/support interactions established by this trimetallic phase seem to decrease the Ni particle size. Small particles increase the conversions. Another explanation for the increased activity was proposed by Lima *et al.*[34] The formed perovskite phase decomposes during reduction transforming the catalyst into the Ni^0/La_2O_3 form. The metallic Ni then activates the C-H bond leading to dissociation of CH_4 into CH_x and H_x species. The La based support enhances CO_2 adsorption and its dissociation to CO with intermediate formation of $La_2O_2CO_3$. The formed CH_x species also interacts with the mobile lattice oxygen produced at the metal–support interfacial region to form CH_xO adsorbed species. Finally, these species break down to form syngas.[28] A detailed study is required for finding the exact reason for the improved activity of the catalysts. This work is in progress in the author's laboratory.

The mobile oxygen is generated due to the incorporation of other metal into the perovskite lattice.[35] In the case of hydrothermal catalysts, the concentration of Ni in the trimetallic perovskite phase seemed to have increased up to x = 0.6, whereas this phenomenon completed till x = 0.3 in the sol–gel catalysts. This appears to be the major difference in the catalysts prepared by the two methods. Though the conversions of the respective gases were almost the same, in numerical terms the hydrothermal catalyst with x = 0.6 had a slight edge over the sol–gel catalyst with x = 0.3. This may be due to the more amount of Ni perovskite interactions accompanied by higher Ni availability outside the structure in the case of hydrothermal catalysts than in sol–gel catalysts. However, when the catalysts of the same Ni content are compared the sol–gel has an edge over its counterpart. These results are displayed in Table 2.

Higher CO_2 conversion than that of CH_4 observed in the present work suggests that the reforming reaction was accompanied by the reverse water–gas shift (Reaction between H_2 and CO_2 producing CO and H_2O, RWGS) reaction. The H_2/CO ratio, with its value a little lower than 1 also indicates the occurrence of RWGS reaction.

The best catalysts from the two series were selected for the time on stream analysis. Figure 7 illustrates the stability behaviours of the x = 0.6 hydrothermal (Figure 7A) and the x = 0.3 sol–gel (Figure 7B) catalysts. Apparently, the hydrothermal catalyst had exhibited better stability compared to its sol–gel counter-part. The trimetallic phase might have resulted in the formation

Table 2. Activity comparison.

Sl. no.	Catalyst		CH_4 (%)	CO_2 (%)	H_2/CO
1	$LaNi_{0.6}Al_{0.4}O_3$	Hydrothermal	94	97	0.98
		Sol–gel	67	72	0.67
2	$LaNi_{0.3}Al_{0.7}O_3$	Hydrothermal	91	94	0.92
		Sol–gel	93	96	0.97

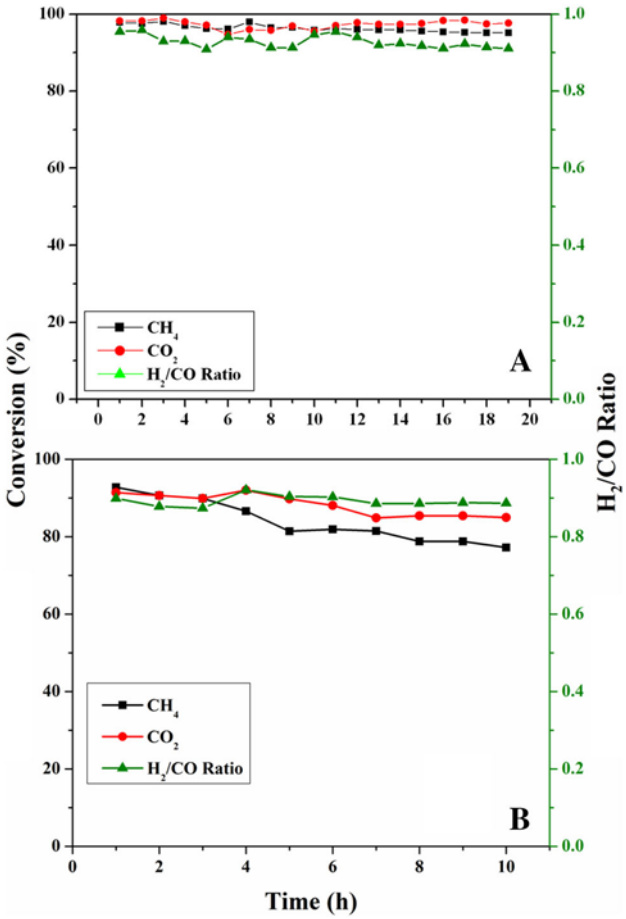

Figure 7. Time on stream study on (A) $LaNi_{0.6}Al_{0.4}O_3$ (Hydrothermal method); (B) $LaNi_{0.3}Al_{0.7}O_3$ (Sol–gel method) at 800°C.

of small Ni particles due to the high dispersion, which prevented ensemble formation leading to increased resistance towards sintering.

Sutthiumporn *et al.*,[36] studied the effect of substitution of Cu and Fe in the perovskite system and found enhanced mobility of lattice oxygen. This oxygen species was found to be the reason for the removal of coke formed during the reforming reaction. A similar phenomenon might have occurred in the present catalysts as well as improving the stability of the catalysts. On the other hand, CO_2 molecules strongly interact with La-based material to form $La_2O_2CO_3$ type species. This phase is highly active to react with carbon deposited on the surface of Ni particles, further decomposing it to CO. The high CO_2 conversion due to its interaction with La oxide support might have increased CO, which in turn reacted with the surface carbon species, thus reducing the overall coke on the catalyst surface.

4. Conclusions

The formation of trimetallic perovskite type oxide phase was confirmed in samples with $0.2 < x < 0.8$ in both hydrothermal and sol–gel catalysts. The trimetallic perovskite is the source for strong Ni-support/structure interaction and eventually for the formation of small sized metal particles that display enhanced catalytic activity. Among the hydrothermal series, $LaNi_{0.6}Al_{0.4}O_3$ exhibited the highest performance, whereas $LaNi_{0.3}Al_{0.7}O_3$ showed superior activity in the sol–gel series. The hydrothermal method of preparation required higher Ni ratio than the sol–gel method for the catalysts to exhibit similar performance. The overall performance of the best hydrothermal catalyst was superior to that of the best sol–gel catalyst, under similar conditions of evaluation over a period of 10 h.

Acknowledgements

The authors thank CSIR and UGC for the financial support in terms of Emeritus Scientist Fellowship and Senior Research Fellowship.

References

1. Lim Y, Lee C J, Jeong Y S, Song I H, Lee C J and Han C 2012 Optimal design and decision for combined steam reforming process with dry methane reforming to reuse CO_2 as a raw material *Ind. Eng. Chem. Res.* **51** 4982
2. Wang W, Su C, Wu Y, Ran R and Shao Z 2013 Progress in solid oxide fuel cells with nickel-based anodes operating on methane and related fuels *Chem. Rev.* **113** 8104
3. Upendar K, Sagar T V, Raveendra G, Lingaiah N, Rao B V, Prasad R B N and Sai Prasad P S 2014 Development of a low temperature adsorbent from karanja seed cake for CO_2 capture *RSC Adv.* **4** 7142
4. Shi L, Yang G, Tao K, Yoneyama Y, Tan Y and Tsubaki N 2013 An introduction of CO_2 conversion by dry reforming with methane and new route of low-temperature methanol synthesis *Acc. Chem. Res.* **46** 1838

5. Daza Y A, Kent R A, Yung M M and Kuhn J N 2014 Carbon dioxide conversion by reverse water–gas shift chemical looping on perovskite-type oxides *Ind. Eng. Chem. Res.* **53** 5828
6. Kumar M A, Venumadhav C, Sagar T V, Surendar M, Lingaiah N, Rao G N and Prasad P S 2014 Catalytic tri-reforming of glycerol for hydrogen generation *Indian J. Chem. Sect. B* **53A** 530
7. Wang S and (Max) Lu G Q 1999 A comprehensive study on carbon dioxide reforming of methane over Ni/ γ-Al_2O_3 catalysts *Ind. Eng. Chem. Res.* **38** 2615
8. Tian L, Zhao X H, Liu B S and Zhang W D 2009 Preparation of an industrial Ni-based catalyst and investigation on CH_4/CO_2 reforming to syngas *Energy Fuels* **23** 607
9. Wang S and Lu G Q 1998 Catalytic activities and coking characteristics of oxides-supported Ni catalysts for CH_4 reforming with carbon dioxide *Energy Fuels* **12** 248
10. Sierra Gallego G, Batiot-Dupeyrat C, Barrault J and Mondragón F 2008 Dual active-site mechanism for dry methane reforming over Ni/La_2O_3 produced from $LaNiO_3$ perovskite *Ind. Eng. Chem. Res.* **47** 9272
11. Olsbye U, Wurzel T and Mleczko L 1997 Kinetic and reaction engineering studies of dry reforming of methane over a $Ni/La/Al_2O_3$ catalyst *Ind. Eng. Chem. Res.* **36** 5180
12. Lee J H, Lee E G, Joo O S and Jung K D 2004 Stabilization of Ni/Al_2O_3 catalyst by Cu addition for CO_2 reforming of methane *Appl. Catal. A Gen.* **269** 1
13. Das T and Deo G 2012 Promotion of alumina supported cobalt catalysts by iron *J. Phys. Chem. C* **116** 20812
14. Kathiraser Y, Thitsartarn W, Sutthiumporn K and Kawi S 2013 Inverse $NiAl_2O_4$ on $LaAlO_3 - Al_2O_3$: unique catalytic structure for stable CO_2 reforming of methane *J. Phys. Chem. C* **117** 8120
15. Zhu T and Flytzani-Stephanopoulos M 2001 Catalytic partial oxidation of methane to synthesis gas over $Ni - CeO_2$ *Appl. Catal. A Gen.* **208** 403
16. Wang N, Shen K, Huang L, Yu X, Qian W and Chu W 2013 Facile route for synthesizing ordered mesoporous Ni–Ce–Al oxide materials and their catalytic performance for methane dry reforming to hydrogen and syngas *ACS Catal.* **3** 1638
17. Chen H W, Wang C Y, Yu C H, Tseng L T and Liao P H 2004 Carbon dioxide reforming of methane reaction catalyzed by stable nickel copper catalysts *Catal. Today* **97** 173
18. Bradford M C and Vannice M A 1999 CO_2 reforming of CH_4 *Catal. Rev. Sci. Eng.* **41** 1
19. Moradi P and Parvari M 2006 Preparation of Lanthanum–Nickel–Aluminium perovskites system and their application in methane reforming reactions *Iran. J. Chem. Eng.* **3** 29
20. Sagar T V, Sreelatha N, Hanmant G, Surendar M, Lingaiah N, Rao K R, Satyanarayana C V, Reddy I A and Prasad P S 2014 Influence of method of preparation on the activity of La–Ni–Ce mixed oxide catalysts for dry reforming of methane *RSC Adv.* **4** 50226
21. Sagar T V, Sreelatha N, Hanmant G, Upendar K, Lingaiah N, Rao K S, Satyanarayana CV, Reddy I A and Prasad P S 2014 Methane reforming with carbon dioxide over $La\text{-}Ni_x - Ce_{1-x}$ mixed oxide catalysts *Indian J. Chem. Sect. A* **53A** 478
22. Khalesi A, Arandiyan H R and Parvari M 2008 Effects of lanthanum substitution by strontium and calcium in La–Ni–Al perovskite oxides in dry reforming of methane *Chin. J. Catal.* **29** 960
23. Khalesi A, Arandiyan H R and Parvari M 2008 Production of syngas by CO_2 reforming on $M_xLa_{1-x}Ni_{0.3}Al_{0.7}O_{3-d}$ (M = Li, Na, K) catalysts *Ind. Eng. Chem. Res.* **47** 5892
24. Li J, Wang D, Zhou G, Xue Y, Li C and Cheng T 2011 Role of A (A= Ca, Mg, Sr) over hexaaluminates $La_{0.8}A_{0.2}NiAl_{11}O_{19}$ for carbon dioxide reforming of methane *Ind. Eng. Chem. Res.* **50** 10955
25. Provendier H, Petit C, Estournes C, Libs S and Kiennemann A 1999 Stabilisation of active nickel catalysts in partial oxidation of methane to synthesis gas by iron addition. *Appl. Catal. A Gen.* **180** 163
26. Rida K, Peña M A, Sastre E and Martinez-Arias A 2012 Effect of calcination temperature on structural properties and catalytic activity in oxidation reactions of $LaNiO_3$ perovskite prepared by Pechini method *J. Rare Earth* **30** 210
27. Moradi G R, Khosravian F and Rahmanzadeh M 2012 Effects of partial substitution of Ni by Cu in $LaNiO_3$ perovskite catalyst for dry methane reforming *Chin. J. Catal.* **33** 797
28. Valderrama G, Goldwasser M R, de Navarro C U, Tatibouët J M, Barrault J, Batiot-Dupeyrat C and Martínez F 2005 Dry reforming of methane over Ni perovskite type oxides *Catal. Today* **107** 785
29. Pereñiguez R, Gonzalez-delaCruz V M, Caballero A and Holgado J P 2012 $LaNiO_3$ as a precursor of Ni/La_2O_3 for CO_2 reforming of CH_4: effect of the presence of an amorphous NiO phase *Appl. Catal. B Environ.* **123** 324
30. Moriga T, Usaka O, Imamura T, Nakabayashi I, Matsubara I, Kinouchi T, Kikkawa S and Kanamaru F 1994 Synthesis crystal structure, and properties of oxygen-deficient lanthanum nickelate $LaNiO_{3-x}$ ($0 \leq x \leq 0.5$) *Bull. Chem. Soc. Jpn.* **67** 687
31. Zhou D, Huang G, Chen X, Xu J and Gong S 2004 Synthesis of $LaAlO_3$ via ethylenediaminetetraacetic acid precursor *Mater. Chem. Phys.* **84** 33
32. Hassanzadeh-Tabrizi SA and Taheri-Nassaj E 2011 Synthesis of high surface area $Al_2O_3-CeO_2$ composite nanopowder via inverse co-precipitation method *Ceram. Int.* **37** 1251
33. Couzi M and Huong P V 1972 Spectres infrarouges des perovskites de terres rares LZO_3 (Z= Al, Cr, Fe, Co) *J. Chim. Phys*. **69** 1339
34. Lima S M, Assaf J M, Pena M A and Fierro J L G 2006 Structural features of $La_{1-x}Ce_xNiO_3$ mixed oxides and performance for the dry reforming of methane *Appl. Catal. A Gen.* **311** 94
35. Sutthiumporn K 2011 In *Development of Nickel Based Catalysts Synthesized Over Different Precursors for Dry* CO_2 *Reforming of Methane to Syngas Production* (Singapore: National University Of Singapore) p. 94
36. Sutthiumporn K, Maneerung T, Kathiraser Y and Kawi S 2012 CO_2 dry-reforming of methane over $La_{0.8}Sr_{0.2}Ni_{0.8}M_{0.2}O_3$ perovskite (M= Bi, Co, Cr, Cu, Fe): roles of lattice oxygen on C–H activation and carbon suppression *Int. J. Hydrogen Energy* **37** 11195